DFT insight into Cd^{2+}, Hg^{2+}, Pb^{2+}, Sn^{2+}, As^{3+}, Sb^{3+}, and Cr^{3+} heavy metal ions adsorption onto surface of bowl-like B_{30} nanosheet

Sadegh Kaviani, Dmitrii A. Tayurskii, Oleg V. Nedopekin, Irina Piyanzina

Institute of Physics, Kazan Federal University, 420008 Kazan, Russia

ABSTRACT

Contamination of water resources by heavy metal ions, is a drastic environmental concern. In this study, the interaction of Cd^{2+}, Hg^{2+}, Pb^{2+}, Sn^{2+}, As^{3+}, Sb^{3+}, and Cr^{3+} metal ions onto surface of the bowl-like B_{30} nanosheet was scrutinized based on density functional theory (DFT) calculations. Adsorption energy (E_{ads}) values revealed that the As^{3+} interacted better with bowl-like B_{30} nanosheet in comparison to other metal ions, having adsorption energy values of -299.57 and -628.56 kcal mol^{-1} in the gas phase and aqueous media, respectively. However, Hg^{2+}, Pb^{2+}, and Sn^{2+} metal ions physically adsorbed onto bowl-like B_{30} nanosheet in the gas phase because of their much less value of adsorption energy. The sign of adsorption Gibbs free energy change (ΔG_{ads}) and adsorption enthalpy change (ΔH_{ads}) values for all complexes was found to be negative in the gas phase and aqueous media, which indicated that the adsorption process is spontaneous and exothermic. Frontier molecular orbital (FMO) analysis exhibited a decrease in the HOMO-LUMO energy gap of studied complexes, boosting the electrical conductivity of these complexes. Natural bond orbital (NBO) analysis and charge decomposition analysis (CDA) revealed donor–acceptor charge transfer interactions in the complexes. The UV–vis results depicted that λ_{max} was red-shifted during interactions of meal ions with bowl-like B_{30} nanosheet. Finally, quantum theory of atoms in molecules (QTAIM) exhibited that the interaction between As^{3+} metal ion and the nanosheet is covalent in nature, while the other metal ions have predominantly electrostatic with partially covalent and non-covalent characters. The theoretical results of the study represented the feasibility of applying bowl-like B_{30} nanosheet to remove heavy metal ions, especially As^{3+} and providing information for experimental researchers to treat wastewaters.

1. Introduction

Anthropogenic activities have been led to the aggregation of heavy metal ions such as cadmium (Cd^{2+}), mercury (Hg^{2+}), lead (Pb^{2+}), tin (Sn^{2+}), arsenic (As^{3+}), antimony (Sb^{3+}), and chromium (Cr^{3+}) in the environment [1,2]. Heavy metal ions can quickly enter the food cycle through various pathways and cause long-term damaging some body tissues, resulting in oxidative stress and then progressive disorders such as cancer [3], neurodegenerative [4], pulmonary [5], and cardiovascular diseases [6]. Unlike some organic contaminants, heavy metal ions are non-biodegradable and can not be decomposed or metabolized. Hence, reliable techniques are indispensable to detect and adsorb the heavy metal ions from wastewaters, especially industrial effluents [7].

Conventional techniques, including solvent extraction [8], coagulation [9], ion-exchange [10], chemical precipitation [11], membrane filtration [12], and reverse osmosis [13] have been utilized

for the remediation of environmental biological samples. However, these techniques possess high cost and low efficiency when there is a lower concentration of heavy metal ions in wastewaters [14]. Among various techniques, adsorption process is highlighted as one of the impressive methods of heavy metal ion removal, because of its simplicity, convenience, effectiveness, and appropriate cost [15–18]. Furthermore, some adsorption methods are reversible and adsorbent can be reutilized after passing desorption. A number of efficient adsorbents have been prepared and used for the removal of toxic metal ions from wastewaters [19]. The conventional adsorbents such as silica, clay minerals, chitosan, zeolites, activated carbons, and polymers suffer from feeble metal ion binding affinity, instability, and low capacity for metal ion removal [14].

Nanomaterials are the most desirable for the heavy metal ion removal due to their inimitable properties, including large surface to the volume ratio, great biocompatibility, small size, surface modifiability, separation facility, high adsorption capacity, accuracy, and reactivity [20–25]. Hence, scientific communities have

paid a lot of attention to design adsorbents based nanostructured materials for biological applications. Boron-based nanomaterials are environmentally benign materials, which have developed in the field of various sensing and adsorption due to great physical and chemical properties such as electrical insulation, high specific surface area (SSA), wide energy band gap, high thermal conductivity, and stability [26]. Because of the electron deficiency of boron element, it is able to form strong covalent bonds with itself and other elements in the periodic table. A nanosheet containing quasi-planar all-boron and a central pentagonal ring so-called bowl-like B_{30} nanosheet has been studied by Wang et al [27]. Their results showed that the bowl-like B_{30} nanosheet as an analogue of corannulene ($C_{20}H_{10}$), was found to have C5v symmetry and built up by addition of two strings of 10 and 15 boron atoms . The bonding and structures of several boron clusters have been studied theoretically and experimentally up to B_{27} and B_{25} using photoelectron spectroscopy and ion mobility, respectively [28]. It has been revealed that the bowl-like B_{30} nanosheet is a two dimensional structure with hexagonal vacancies [29]. This suggests indirect experimental sign for the viability of monolayer-thin boron sheets.

Interaction of metal ions and organic molecules with the surface of boron- based nanomaterials is of great significance due to its possible applications in electrochemical sensors [30], wastewater treatment [31–35], and hydrogen storages [36]. Based on a theoretical investigation by Azamat et al., boron nitride (BN) nanosheets can effectively adsorb Cu^{2+} and Hg^{2+} heavy metal ions from aqueous solutions [37]. In another work performed by Han et al., the adsorption mechanisms of Cu^{2+}, Cd^{2+}, and Ni^{2+} metal ions on BN were experimentally investigated. They concluded that adsorption appears to be much fast (<2 min) with a removal order of $Cu^{2+} > Cd^{2+} > Ni^{2+}$ [38]. Milon et al. have performed theoretical calculations on the B_6 nanocluster as an adsorbent of W^{6+}, Cd^{2+}, Cr^{2+} heavy metal ions in the aqueous environment [39]. The adsorption energies demonstrated that the complex clusters are formed through chemisorption process and this is desirable for removal of heavy metal ions. Li et al. used BN nanosheets to look into adsorption properties of Pb^{2+}, Cr^{3+}, and Hg^{2+} metal ions using experimental and theoretical methods [40]. They found that the activated porous boron nitride nanosheets may be considered as an efficient activated carbon material for the removal of the metal ions from the wastewater. Based on Azamat et al. results, BN nanosheet could successfully separate Cd^{2+} and Pb^{2+} metal ions from water [41]. However, few theoretical studies have been conducted into environmental and biological applications of bowl-like B_{30} nanosheet [42,43].

In this study, we have studied the adsorption properties of Cd^{2+}, Hg^{2+}, Pb^{2+}, Sn^{3+}, As^{3+}, Sb^{3+}, and Cr^{3+} heavy metal ions onto bowl-like B_{30} nanosheet using density functional theory (DFT) method. In order to do a systematic computational study, bowl-like B_{30} nanosheet and its metal complexes was also considered in water as an aqueous media. The structural stability along with their thermodynamic, electronic and optical properties has been investigated for the better insight of the adsorption process. The aim of this study is motivating future research studies into the application of the bowl-like B_{30} nanosheet as a novel chemical sensor to detect and adsorb some toxic heavy metal ions in aqueous media.

2. Computational details

Gaussian 16 program package was used to carry out the DFT calculations [44]. Optimization of all structures was carried out at the ωB97XD level of theory. A review of the literature reveals that the ωB97XD (dispersion-corrected van der Waals functional) is a suitable and reliable level for predicting the geometrical, electronic, optic, and energetic properties of various boron-based

nanostructures as well as adsorption studies [45–48]. The LanL2DZ [49,50] basis set was used for Cd^{2+}, Hg^{2+}, Pb^{2+}, Sn^{2+}, As^{3+}, Sb^{3+}, and Cr^{3+} metal ions, while the 6–31g(d,p) [51–53] has been utilized for the boron atoms. All properties of Cd^{2+}, Hg^{2+}, Pb^{2+}, Sn^{2+}, As^{3+}, and Sb^{3+} complexes were calculated for the singlet ground state whereas Cr^{3+} complex has the quartet ground state. Vibrational frequencies were evaluated to find the ground-state local minima structures. It should be noted that there were not any imaginary frequencies, demonstrating the optimized structures are in true minimum potential energy and can be possible to synthesis.

The adsorption energy (E_{ad}) for the metal ion interaction with the bowl-like B_{30} nanosheet was calculated by the Eq (1).

$$E_{ads} = E_{M/B_{30}} - (E_{B_{30}} + E_M) + E_{BSSE} \qquad (1)$$

Where $E_{M/B_{30}}$ is the total energy of the M^{2+}/B_{30} and M^{3+}/B_{30} complexes system, $E_{B_{30}}$ stands for the total energy of the bowl-like B_{30} nanosheet and E_M represents the total energy of the adsorbed metal ions. E_{BSSE} is the basis set superposition error in the adsorption energy, which was corrected by using the counterpoise (CP) method [54]. Also, the thermodynamic parameters such as Gibbs free energy (ΔG), enthalpy (ΔH), and entropy (ΔS) were calculated at P = 1 atm and T = 298.15 K by the Eqs (2–4), respectively.

$$\Delta G_{ads} = \Delta G_{M/B_{30}} - (\Delta G_{B_{30}} + \Delta G_M) \qquad (2)$$

$$\Delta H_{ads} = \Delta H_{M/B_{30}} - (\Delta H_{B_{30}} + \Delta H_M) \qquad (3)$$

$$\Delta S_{ads} = \frac{(\Delta H_{ads} - \Delta G_{ads})}{T} \qquad (4)$$

To investigate the aqueous media effects on adsorption energies, the polarizable continuum model (PCM) was applied as the default SCRF (Self-Consistent Reaction Field) method [55]. For this purpose, water was applied as an aqueous media with dielectric constant of 78.54 at T = 298.15 K. Furthermore, the solvation energy (ΔE_{sol}) was calculated to understand the stability and solubility of M^{2+}/B_{30} and M^{3+}/B_{30} complexes in aqueous media by the Eq (5) [56].

$$\Delta E_{sol} = E_{aqu} - E_{gas} \qquad (5)$$

In this equation, E_{aqu} and E_{gas} stand for the total energy of the complexes in the aqueous media and gas phase, respectively.

To get confirmation of the adsorption of metal ions on bowl-like B_{30} nanosheet, we have also investigated sensitivity of the adsorbents towards metal ions using electronic properties such as the energy of highest occupied molecular orbital (E_{HOMO}), the energy of lowest unoccupied molecular orbital (E_{LUMO}), density of states (DOS), and UV–vis spectra. In order to obtain more information about chemical stability and reactivity of the structures, quantum molecular descriptors such as chemical hardness (η), electronic chemical potential (μ), and electrophilicity index (ω) were calculated by means of the Eqs (6–8), respectively [57,58].

$$\eta = \frac{E_{LUMO} - E_{HOMO}}{2} \qquad (6)$$

$$\mu = -\frac{(E_{LUMO} + E_{HOMO})}{2} \qquad (7)$$

$$\omega = \frac{\mu^2}{2\eta} \qquad (8)$$

Natural bond orbital (NBO) [59] analysis and charge decomposition analysis (CDA) [60] analysis were conducted to analyze the relative strength of the donor-accepter interactions in terms of charge transfer. Quantum theory of atoms in molecules (QTAIM) [61] was also performed to investigate the nature of interactions

in M^{2+}/B_{30} and M^{3+}/B_{30} complexes. The CDA and QTAIM analyses were measured by Multiwfn 3.1 software [62]. For all optimized structures, time dependent density functional theory (TD-DFT) calculations [63,64] were carried out to obtain UV–vis spectra. In these calculations, excitations to the first 20 singlet excited states were considered and two different functional namely ωB97XD [65] and B3LYP [66] were used for calculations of the absorption spectra with the same basis set for geometry optimization.

3. Results and discussion

3.1. Structural analysis

First, the bare structure of the bowl-like B_{30} nanosheet has been optimized geometrically at ωB97XD exchange correlation functional as well as 6–31g(d,p) basis set. The optimized structure and geometrical parameters are shown in Fig. 1 and Table S1, respectively The bowl-like B_{30} nanosheet consists a pentagonal ring (B5) and two rings around it (B10 and B15) respectively. As revealed in Table S1, the values of the B − B bond distances are in good agreement with the previous DFT calculation performed on bowl-like B_{30} nanosheet by Rahimi and Solimannejad [43]. Fig. 2 shows all the M^{2+}/B_{30} and M^{3+}/B_{30} relaxed structures in the gas phase, which have been optimized by ωB97XD level of theory. The possible adsorption sites of bowl-like B_{30} nanosheet known as internal and external sites are examined to obtain the most stable complex of the adsorbed metal ions onto surface of the bowl-like B_{30} nanosheet. The results indicate that the most possible location for adsorption of metal on the bowl-like B_{30} nanosheet is hollow pentagonal ring (internal site) as shown in Fig. 2. The calculated B − M bond length values for M^{2+}/B_{30} and M^{3+}/B_{30} complexes are summarized in Table S1. After the full relaxation of the complexes, M − B bond distances of free bowl-like B_{30} nanosheet increase slightly. According to Table S1, M − B bond distances decrease in aqueous media compared to the gas phase. Moreover, the As − B bond distance of As^{3+}/B_{30} complex is equal to be 2.27 Å in the aqueous media, which is the lowest amount. This reveals that the As^{3+} metal ion has better interaction with the bowl-like B_{30} nanosheet in comparison to other metal ions. The graphical representation of change in the M − B bond distances with the change in ionic radii of metals is shown in Fig. 3. Based on this figure, the M − B bond distances increase with enhancing the ionic radii values in the gas phase and aqueous media.
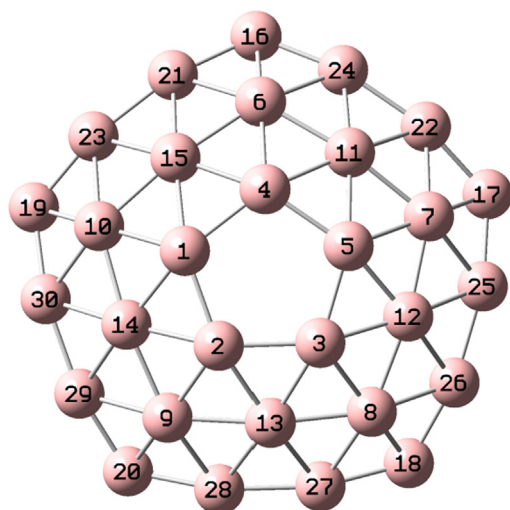

Fig. 1. Optimized geometry of bowl-like B_{30} nanosheet in the gas phase.

3.2. Adsorption energy and thermodynamic analysis

Before calculating the adsorption energy of the M^{2+}/B_{30} and M^{3+}/B_{30} complexes, cohesive formation energy (E_{Coh}) of the bowl-like B_{30} nanosheet are computed, which gives the information about the stability and durability of the free nanosheet. The cohesive formation energy has been calculated with the help of Eq (9) [67–69].

$$E_{Coh} = \frac{1}{n}(E_{B_{30}} - nE_B) \tag{9}$$

Where n is the number of atoms in bowl-like B_{30} nanosheet, E_{B30} and E_B are the total energy of the bowl-like B_{30} nanosheet and energy each boron atom, respectively. The calculated cohesive formation energy per atoms of bowl-like B_{30} nanosheet is found to be negative (-118.67 kcal mol^{-1}), which guarantee the stability of the nanosheet. The adsorption energy (E_{ads}) is a measure of system stability such that more negative value of E_{ads} gives more stability of a nanostructure [70]. The calculated adsorption energies of two and three positively-charged metal ions (M^{2+} and M^{3+}, respectively) are summarized in Tables 1 and 2, respectively. The negative value of E_{ads} for all complexes shows that they are stable with energetically favorable in both gas and aqueous media. The much more negative adsorption energy values in the aqueous media demonstrate that bowl-like B_{30} nanosheet can be an excellent metal ion adsorbent in aqueous media. Hydration of nanosheet and metal ions in water media leads to the large adsorption energy value difference in the gas phase and water media. Calculated E_{ads} values of simulated M^{2+}/B_{30} and M^{3+}/B_{30} complexes in the gas phase and aqueous media show that the stability trend is as follows: As^{3+} > Cr^{3+} > Sb^{3+} > Cd^{2+} > Hg^{2+} > Sn^{2+} > Pb^{2+}. From this presented trend, we can conclude that As^{3+} metal ion adsorbed on bowl-like B_{30} nanosheet is the most stable one. Besides, the weak interactions are observed with the Sn^{2+}, Pb^{2+} and Hg^{2+} metal ions in the gas phase, which have the lowest adsorption energies of −6.15, −2.79, and −8.09 kcal mol^{-1} and can be characterized as physisorption process because of much lower adsorption energy values r than –23 kcal mol^{-1} [71].

Thermodynamic parameters including changes in enthalpy (ΔH), changes in Gibbs free energy (ΔG), and changes in entropy (ΔS), were also scrutinized and reported in Tables 1 and 2. Based on these data, the character of the adsorption process of metal ions onto bowl-like B_{30} nanosheet is exothermic because of negative values of ΔH_{ads}, which is suitable in metal ion adsorption applications. Negative values of ΔS_{ads} are observed for all structures since the atom movement is confined because of the appearance of the metal ions and newly formed intermolecular bonds. The negative values of ΔG_{ads} clearly reveal that the adsorption of metal ion onto bowl-like B_{30} nanosheet is spontaneous in nature. Furthermore, the decline in the amount of ΔG_{ads} compared to ΔH_{ads} can be justified by considering the entropic effects [72]. Fig. 4 represents the correlation between metal ions and adsorption energies in the gas phase and aqueous media. Here, we see that adsorption energy increases linearly with increase of the ionic radii of metals.

3.3. NBO analysis and CDA

NBO analysis provides useful information about intermolecular interactions and hybridization through charge transfer between adsorbate and adsorbent. The stabilization energy is evaluated by using second-order perturbation theory and the associated delocalization of charges from donor (i) to acceptor (j) is calculated by Eq (10) [73,74].
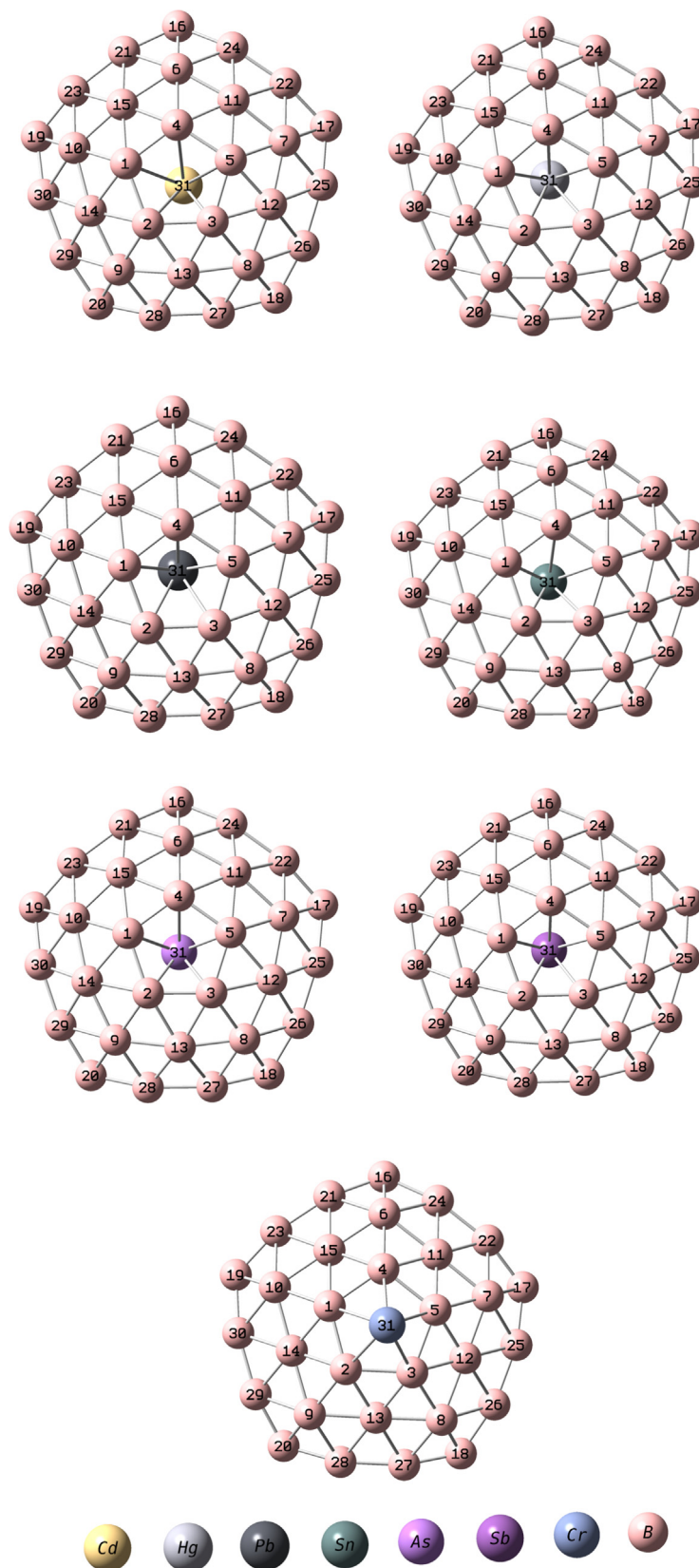
$$E^2 = q_i \frac{F_{ij}^2}{E_j - E_i} \tag{10}$$

Fig. 2. Optimized structures of metal ion adsorbed onto bowl-like B$_{30}$ nanosheet in the gas phase.

In the above equation, E$_i$ and E$_j$ denote the orbital energies of the complexes, q$_i$ and F$_{ij}$ are the donor orbital occupancy and off-diagonal element of the NBO Fock matrix, respectively.

It is possible to compare the stability of different complexes by the calculation of the stabilization energy E(2), such that a higher value of E(2) implies that a significant amount of electron density
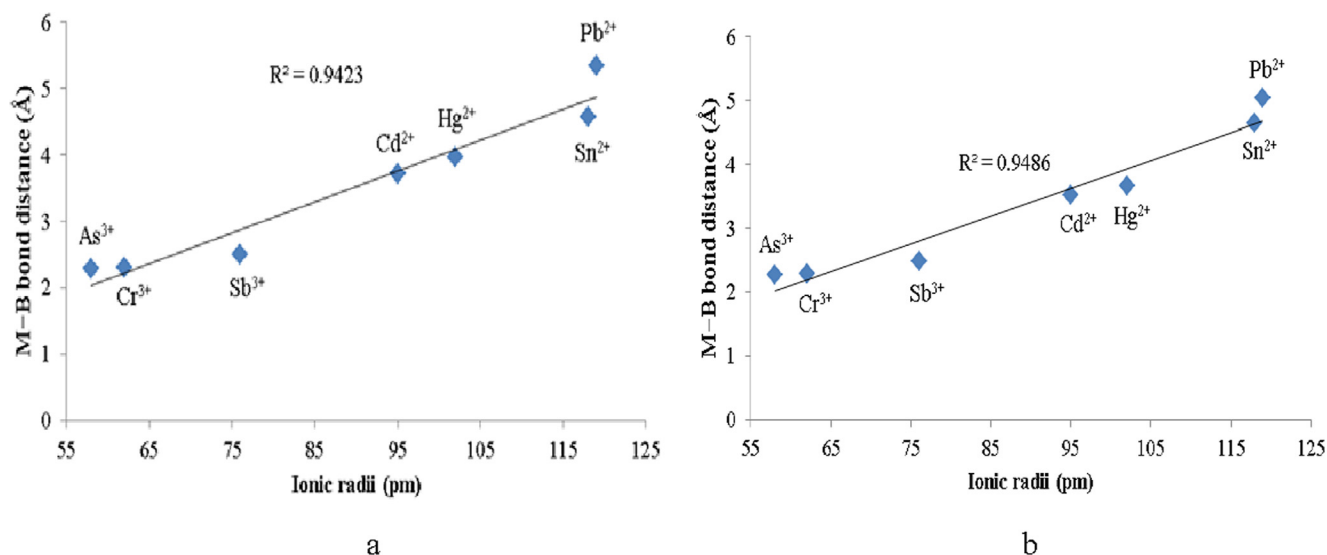
Fig. 3. Graphical representation of the relationship between the M − B bond distance and the ionic radii of metals in the a) gas phase and b) aqueous media.

Table 1
The calculated adsorption (E_{ads}), changes of adsorption Gibbs energy (ΔG_{ads}), enthalpy (ΔH_{ads}) in kcal mol^{-1}, and entropy (ΔS_{ads}) in kcal mol^{-1} K^{-1} for M^{2+}/B$_{30}$ complexes in the gas phase and aqueous media.

M^{2+}	Media	E_{ads}	BSSE	$E_{ads,CP}$	ΔG_{ads}	ΔH_{ads}	ΔS_{ads}
Cd^{2+}	Gas	−55.24	5.68	−49.56	−46.83	−55.81	−0.030
	Water	−203.50	5.75	−197.75	−198.10	−204.12	−0.020
Hg^{2+}	Gas	−9.22	1.13	−8.09	−6.19	−9.78	−0.012
	Water	−171.14	1.44	−169.70	−162.30	−177.64	−0.051
Pb^{2+}	Gas	−3.95	1.16	−2.79	−3.26	−4.52	−0.004
	Water	−141.25	1.29	−139.96	−133.03	−141.81	−0.029
Sn^{2+}	Gas	−7.34	1.19	−6.15	−5.58	−7.90	−0.023
	Water	−161.89	1.25	160.64	−153.55	−161.28	−0.025

Table 2
The calculated adsorption (E_{ads}), changes of adsorption Gibbs energy (ΔG_{ads}), enthalpy (ΔH_{ads}) in kcal mol^{-1}, and entropy (ΔS_{ads}) in kcal mol^{-1} K^{-1} for M^{3+}/B$_{30}$ complexes in the gas phase and aqueous media.

M^{3+}	Media	E_{ads}	BSSE	$E_{ads,CP}$	ΔG_{ads}	ΔH_{ads}	ΔS_{ads}
As^{3+}	Gas	−299.57	8.67	290.90	−290.41	−300.20	−0.033
	Water	−628.56	8.92	619.64	−619.41	−629.07	−0.032
Sb^{3+}	Gas	−220.62	5.45	215.17	−211.39	−222.38	−0.036
	Water	−469.94	5.64	464.30	−460.96	−470.44	−0.032
Cr^{3+}	Gas	−292.74	8.79	283.95	−284.40	−293.24	−0.029
	Water	−611.51	9.04	−602.47	−603.79	−612.07	−0.028

is delocalized from donor to acceptor and greater stability is attained. NBO analysis is performed for metal ions over free bowl-like B$_{30}$ nanosheet in aqueous media and the corresponding results are given in Table 3. Based on this table, charge is transferred from bowl-like B$_{30}$ nanosheet to the metal ions. Boron atom of bowl-like B$_{30}$ nanosheet behaves like a good electric charge donor and binds to the electron rich metal ion through highly stable M − B bonds. It is notable that with going from As^{3+} as the smallest metal ion to Pb^{2+} as the largest one, the Σ E^2 values decreases from 527.08 to 14.07 kcal mol^{-1} (see Fig. 5). This shows that the lower ionic radii of metals results in the stronger donor–acceptor interaction energy.

The CDA is an unraveling method for the assessment of the relative strength of charge donation (d) and back-donation (b) in the complex. The CDA results are reported in Table 4. Here, the relative amounts of forward-donation, back-donation and repulsion are considered in the M^{2+}/B$_{30}$ and M^{3+}/B$_{30}$ complexes. The relative total charge transfer values (d-b) of −0.426 esu, −0.397 esu, −0.250 esu, −0.292 esu, −0.530 esu, −0.492 esu, and −0.495 esu are observed in Cd^{2+}/B$_{30}$, Hg^{2+}/B$_{30}$, Pb^{2+}/B$_{30}$, Sn^{2+}/B$_{30}$, As^{3+}/B$_{30}$, Sb^{3+}/B$_{30}$, and Cr^{3+}/B$_{30}$ complexes, respectively. In Cd^{2+}/B$_{30}$, Hg^{2+}/B$_{30}$, and Pb^{2+}/B$_{30}$ complexes, the charge transfer is more dominated via back-donation from d-orbital of Cd^{2+}, Hg^{2+}, and Pb^{2+} metal ions to p-orbital of B atom, while in other complexes the charge transfer trough donation is dominated over back-donation. The Cd^{2+}, Hg^{2+}, and Pb^{2+} metal ions have d^{10} electronic configuration, and these metal ions don't favor charge transfer trough σ-donation. The repulsive polarization (r) is an important indicator of charge density between donor and acceptor fragments. The values of repulsive polarization in As^{3+}/B$_{30}$, Sb^{3+}/B$_{30}$, and Cr^{3+}/B$_{30}$ complexes are 0.739 esu, 0.764, and 0.596 esu, respectively. These positive values of repulsion indicate that charge density is concentrated in the interaction region between these fragment's pairs. In other fragment's pairs of the complexes the charge density does not accumulate rather it is moving away from the interaction region. Furthermore, an elevation in the ionic radii of metals causes to
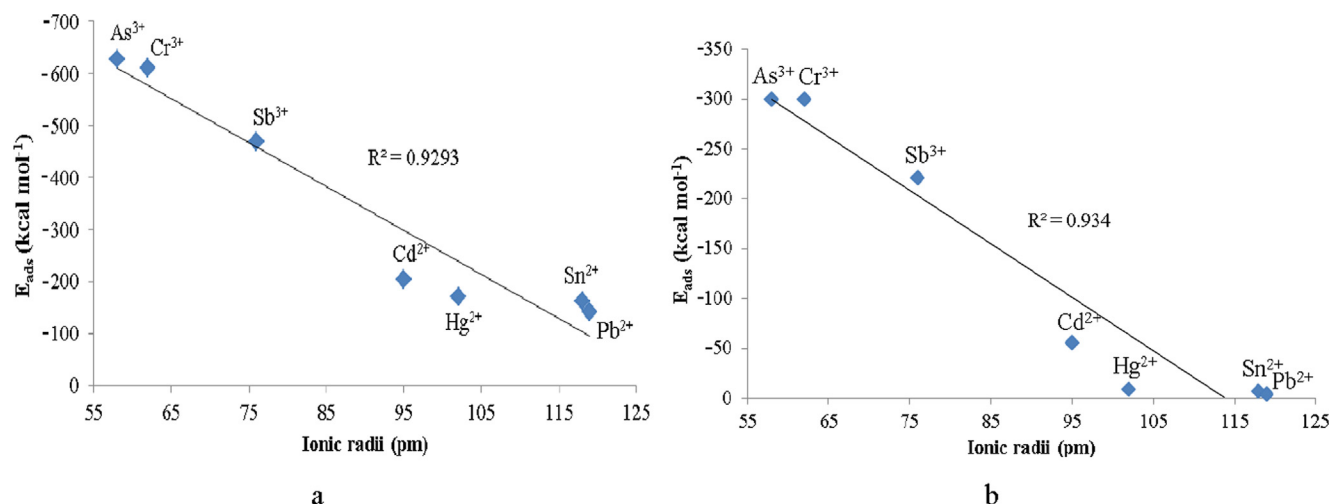
Fig. 4. The relationship between adsorption energy and the ionic radii of metals in the a) gas phase, and b) aqueous media.

Table 3
Most intermolecular charge transfer between bowl-like B_{30} nanosheet and metal ions accompanied with stabilization energies in the aqueous media.

Complex	Donor NBO(i)	Acceptor NBO(j)	E(2) (kcal mol^{-1})	Σ E^2 (kcal mol^{-1})
Cd^{2+}/B$_{30}$	LP*B1	LP*Cd	7.52	68.16
	LP*B2	LP*Cd	33.12	
	LP*B3	LP*Cd	8.35	
	LP*B4	LP*Cd	9.38	
	LP*B5	LP*Cd	9.79	
Hg^{2+}/B$_{30}$	LP*B1	LP*Hg	5.21	45.91
	LP*B2	LP*Hg	21.03	
	LP*B3	LP*Hg	6.04	
	LP*B4	LP*Hg	7.35	
	LP*B5	LP*Hg	6.28	
Pb^{2+}/B$_{30}$	LP*B1	LP*Pb	3.14	14.07
	LP*B2	LP*Pb	4.92	
	LP*B3	LP*Pb	2.04	
	LP*B4	LP*Pb	2.11	
	LP*B5	LP*Pb	1.86	
Sn^{2+}/B$_{30}$	LP*B1	LP*Sn	4.91	24.07
	LP*B2	LP*Sn	10.22	
	LP*B3	LP*Sn	5.12	
	LP*B4	LP*Sn	1.27	
	LP*B5	LP*Sn	2.55	
As^{3+}/B$_{30}$	LP*B1	LP*As	91.96	527.08
	LP*B2	LP*As	102.69	
	LP*B3	LP*As	139.70	
	LP*B4	LP*As	89.11	
	LP*B5	LP*As	103.62	
Sb^{3+}/B$_{30}$	LP*B1	LP*Sb	60.63	359.80
	LP*B2	LP*Sb	61.34	
	LP*B3	LP*Sb	117.29	
	LP*B4	LP*Sb	59.77	
	LP*B5	LP*Sb	60.77	
Cr^{3+}/B$_{30}$	LP*B1	LP*Cr	83.47	446.55
	LP*B2	LP*Cr	81.22	
	LP*B3	LP*Cr	119.56	
	LP*B4	LP*Cr	81.03	
	LP*B5	LP*Cr	81.27	

decrease the total charge transfer between the metal ion and bowl-like B_{30} nanosheet, which is represented by linear regression analysis for all investigated complexes (see Fig. 6).

3.4. Frontier molecular orbitals (FMOs) and quantum molecular descriptors

The interaction mechanism of metal ion on the surface of an adsorbent is described through the frontier molecular orbital theory [75]. The band gap (E_g) is an electronic parameter to assess the electrical conductivity (σ) of an adsorbent toward an adsorbate based on the Eq (11).

$$\sigma = AT^{\frac{3}{2}}exp(\frac{-E_g}{2kT})$$ (11)

where k refers to Boltzmann's constant, T denotes the temperature in Kelvin, and A is a constant. According to this equation, the conductivity enhances exponentially with a reduction in the HOMO–LUMO energy band gap. This means that an electrical signal can be generated due to the reduction in the HOMO-LUMO energy band
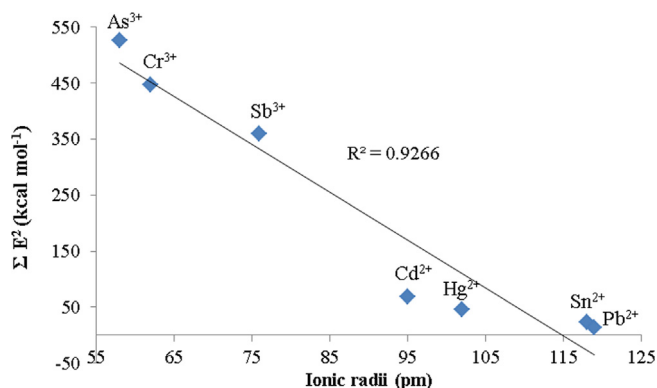
Fig. 5. The change in the second-order perturbation energy with the ionic radii of metals in the aqueous media.

Table 4
CDA analysis for the donation (d), back donation (b), total charge transfer (d-b), and repulsive polarization (r) of M^{2+}/B_{30} and M^{3+}/B_{30} complexes in the aqueous media.

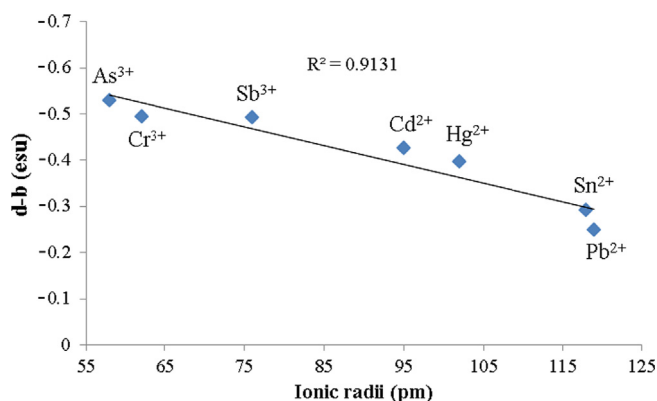| Complex	d	b	d-b	r
Cd^{2+}/B_{30}	−0.068	0.358	−0.426	−0.504
Hg^{2+}/B_{30}	−0.075	0.322	−0.397	−0.701
Pb^{2+}/B_{30}	−0.019	0.231	−0.250	−0.009
Sn^{2+}/B_{30}	−0.207	0.085	−0.292	−0.003
As^{3+}/B_{30}	−0.443	0.087	−0.530	0.739
Sb^{3+}/B_{30}	−0.416	0.076	−0.492	0.764
Cr^{3+}/B_{30}	−0.530	0.035	−0.495	0.596

Fig. 6. The trend of total charge transfer with the ionic radii of metals in the aqueous media.

gap, which is a most important parameter for sensing metal ions and drugs by adsorbents [76–78]. Table 5 shows results regarding HOMO, LUMO energies, their corresponding E_g, and quantum molecular descriptors for bowl-like B_{30} nanosheet, M^{2+}/B_{30} and M^{3+}/B_{30} complexes. The HOMO and LUMO energies of free bowl-like B_{30} nanosheet are to be found −7.45 and −1.52 eV, respectively with observed E_g of 5.93 eV. The adsorption of all metal ions over bowl-like B_{30} nanosheet results in decrease in the E_g values. The results reveal that the sensitivity of the metal ions toward the bowl-like B_{30} nanosheet is as follows: Cd^{2+} > Sn^{2+} >Cr^{3+} > Pb^{2+} > Hg^{2+} > Sb^{3+} > As^{3+}. Therefore, the most prominent decrease in the E_g value is observed in the case of Cd^{2+}/B_{30} complex (2.14 eV), which shows that the Cd^{2+} metal ion is the most sensitive towards bowl-like B_{30} nanosheet among other metal ions. The stability and reactivity of a structure are related to the chemical hardness values, such that the structure with a higher chemical hardness exhibits

higher stability and lower reactivity. The most stable complex is related to As^{3+}/B_{30} complex with the energy gap and chemical hardness values of 5.89 and 2.99 eV, respectively. The larger absolute values of chemical potential are associated with higher chemical reactivity. The calculated chemical potential values for the BN nanosheet and its complexes indicate that after adsorption of Cd^{2+} Hg^{2+} Pb^{2+}, Sn^{2+}, As^{3+}, Sb^{3+}, and Cr^{3+} metal ions, the absolute chemical potential increases from −4.48 to −12.63, −11.68, −12.22, −12.81, −15.03, −14.98, and 15.31 eV, respectively (see Table 5). The electrophilicity index can also be used to investigate the reactivity and toxicity of a structure, in which an increase in the value of electrophilicity index indicates an increase in the chemical reactivity and a decrease in chemical toxicity [75,79]. As seen from the results in Table 5, a significant change can be observed for electrophilicity index values, which shows it is increased about 10–15 times. Therefore, the adsorption of the metal ions increases the capability of the bowl-like B_{30} nanosheet to acquire extra charge from other molecules. This means that the adsorption of the metal ions can lead to inhibit the aggregation of nanosheet and the improvement of its dispersion in biological media. Fig. S1 depicts the HOMO and LUMO of bowl-like B_{30} nanosheet and its metal complexes in the aqueous media. For bowl-like B_{30} nanosheet, the HOMO lies on the entire nanosheet, while the LUMO is situated more over the edge B atoms. The HOMO and LUMO of the Cd^{2+}/B_{30}, Hg^{2+}/B_{30}, Pb^{2+}/B_{30}, and Sn^{2+}/B_{30} complexes are mainly localized on the B atoms. It is clear that the As^{3+}, Sb^{3+}, and Cr^{3+} metal ions adsorbed on the bowl-like B_{30} nanosheet show some different outlook. The HOMO is formed with a higher contribution of metal ion and lower contribution of B_{30} nanosheet, while LUMO is formed with just the contribution of B_{30} nanosheet. This makes more different electronic properties of the As^{3+}/B_{30}, Sb^{3+}/B_{30}, and Cr^{3+}/B_{30} complexes in comparison to other complexes (see Table 5).

To visualize the reduction in the HOMO-LUMO energy gap, the density of states (DOS) spectra were plotted and shown in Fig. S2. After adsorption of metal ions onto bowl-like B_{30} nanosheet, a significant change in the intensity of the peaks is observed. The HOMO and LUMO energy levels of M^{2+}/B_{30} and M^{3+}/B_{30} complexes increase remarkably compared to the free bowl-like B_{30} nanosheet. Thus, the creation of new energy levels and the change in the intensity of the DOS spectra reveal the improving electronic properties accompanied with a reduction in HOMO-LUMO energy gap values.

3.5. Aqueous media effect and dipole moments

In biological systems, the effect of aqueous media on the nanostructure and its performance is of great importance. The capability of bowl-like B_{30} nanosheet to adsorb metal ions in the aqueous media is performed and the solvation energies for all complexes are depicted in Table 6. Bowl-like B_{30} nanosheet and its metal ion complexes show negative ΔE_{sol} values, which indicate the solubility and spontaneity in the aqueous media. The As^{3+}/B_{30} complex has the highest value of solvation energy (-313.75 kcal mol^{-1}), making it most soluble one in the aqueous media. Furthermore, dipole moment (DM) is another essential investigation, which implies the solubility of a system in a polar media like water. The higher value of DM indicates the higher solubility in a polar media [45]. The dipole moment for bowl-like B_{30} nanosheet is found to be 3.80 Debye in the aqueous media. After the adsorption of metal ions onto bowl-like B_{30} nanosheet, the dipole moment of the Cd^{2+}/B_{30}, Hg^{2+}/B_{30}, Pb^{2+}/B_{30}, Sn^{2+}/B_{30}, As^{3+}/B_{30}, Sb^{3+}/B_{30}, and Cr^{3+}/B_{30} complexes are found to be 12.31, 10.82, 10.36, 10.43, 15.70, 14.51, and 14.79 Debye, respectively, which show high polarizability in the aqueous media. A high significant amount of DM was found 15.70 Debye for As^{3+}/B_{30} com-

Table 5

Energies of HOMO (E_{HOMO}) and LUMO (E_{LUMO}), energy gap (E_g), chemical hardness (η), chemical potential (μ), and electrophilicity index (ω) in eV for bowl-like B_{30} nanosheet, and its metal ion complexes in the aqueous media.

System	E_{HOMO}	E_{LUMO}	E_g	η	μ	ω
B_{30}	−7.45	−1.52	5.93	2.96	−4.48	3.39
Cd^{2+}/B_{30}	−14.53	−10.74	3.79	1.89	−12.63	42.19
Hg^{2+}/B_{30}	−14.01	−9.36	4.65	2.25	−11.68	30.31
Pb^{2+}/B_{30}	−14.28	−10.17	4.11	2.05	−12.22	36.42
Sn^{2+}/B_{30}	−14.74	−10.89	3.85	1.92	−12.81	42.73
As^{3+}/B_{30}	−17.98	−12.09	5.89	2.99	−15.03	37.77
Sb^{3+}/B_{30}	−17.55	−12.41	5.14	2.52	−14.98	44.52
Cr^{3+}/B_{30}	−17.32	−13.30	4.02	2.01	−15.31	58.30

Table 6

Calculated solvation energies in kcal mol^{-1} and dipole moment values in Debye for M^{2+}/B_{30} and M^{3+}/B_{30} complexes.

Complex	ΔE_{sol}	DM*
B_{30}	−3.01	6.13
Cd^{2+}/B_{30}	−243.55	12.31
Hg^{2+}/B_{30}	−221.00	10.82
Pb^{2+}/B_{30}	−144.32	10.36
Sn^{2+}/B_{30}	−150.60	10.43
As^{3+}/B_{30}	−313.75	15.70
Sb^{3+}/B_{30}	−309.61	14.51
Cr^{3+}/B_{30}	318.50	14.79

* Dipole moment values were reported in the aqueous media.

plex. Thus, the greatest values of ΔE_{sol} and DM are observed when As^{3+} metal ion interacts with bowl-like B_{30} nanosheet and indicate the highest solubility and stability in the aqueous media. Generally, there is an inverse correlation between dipole moments and solvation energies as plotted in Fig. 7(a). Furthermore, the calculated values of dipole moment decrease with the increase of ionic radii of metals (see Fig. 7(b)).

3.6. UV–vis spectroscopic studies

Excited state calculations are fulfilled with TD-DFT theory for the M^{2+}/B_{30} and M^{3+}/B_{30} complexes in the aqueous media. The results of the calculations and UV–vis spectra of these complexes are given in Table S2 and Fig. S3, respectively. The B3LYP functional are also employed to present the more accurate results for UV–vis spectra calculations [80–82]. The absorption values of the bowl-like B_{30} nanosheet and all the investigated complexes are

in a visible region ranging from 369.22 to 434.05 nm. The observed maximum wavelength of free bowl-like B_{30} nanosheet appeared at 434.05 nm with excitation energy of 2.85 eV, which corresponds to the dominant transition of $H − 1 \rightarrow L + 2$. The adsorption bands of the free bowl-like B_{30} nanosheet move to lower wavelength values after the metal ion adsorption (hypsochromic shift). This shift may be exploited for detecting the concentration of metal ions in the environment. The absorption band with minimum absorption value among all studied complexes is observed in As^{3+}/B_{30} complex at 369.22 nm with $H-1 \rightarrow L + 9$ (40%) HOMO $\rightarrow L + 8$ (44%) transitions as well as excitation energy and oscillator strength of 3.25 eV and 0.138 values, respectively. The incidence of absorption band with higher oscillator strength and lower excitation energy value as appeared in As^{3+}/B_{30} complex is the characteristic of donor–acceptor structures, which is due to the great intermolecular charge transfer and HOMO to LUMO electronic transitions.

3.7. Quantum theory of atoms in molecules analysis

Quantum theory of atoms in molecules analysis is a useful theoretical framework for gaining the precise and more reliable information about strength and nature of the interaction between the metal ion and the proposed bowl-like B_{30} nanosheet. The molecular graph with bond critical points (BCPs) and bond paths are shown in Fig. 8. The existence of BCPs in all complexes indicates the transferring of electron density and confirms the formation of a chemical bond between the bowl-like B_{30} nanosheet and metal ions. In this investigation, some topological parameters such as electron density (ρ_b), Laplacian of electron density ($\nabla^2\rho_b$), kinetic energy density (G_b), potential energy density (V_b) and total energy density (H_b) parameters at BCPs have been calculated and summarized in Table 7. It is possible to classify the strength of
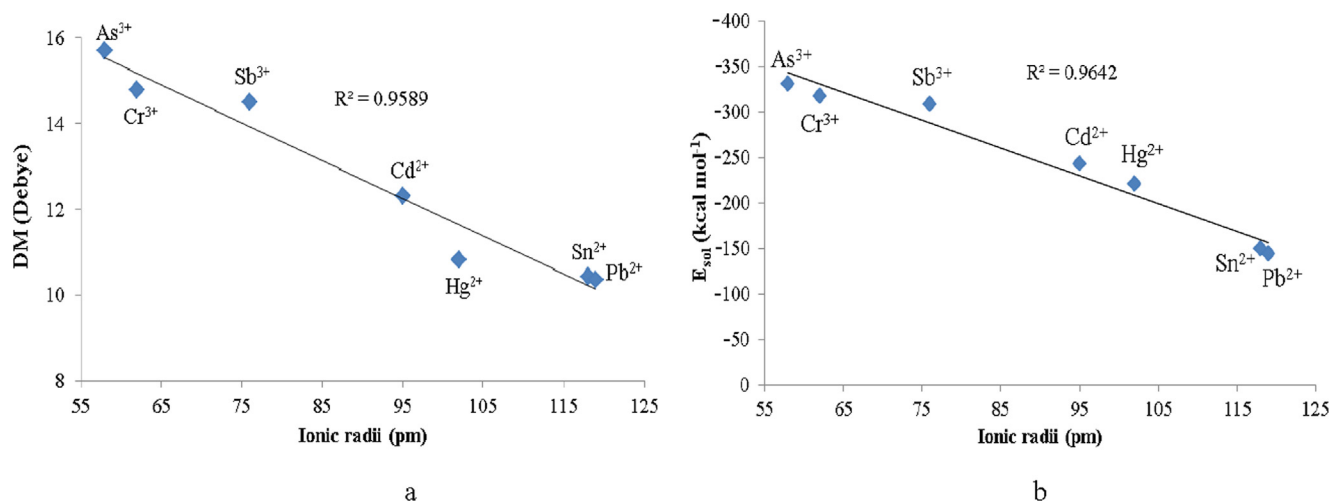

Fig. 7. Linear correlation of a) dipole moment and b) solvation energy with ionic radii of metals in the aqueous media.
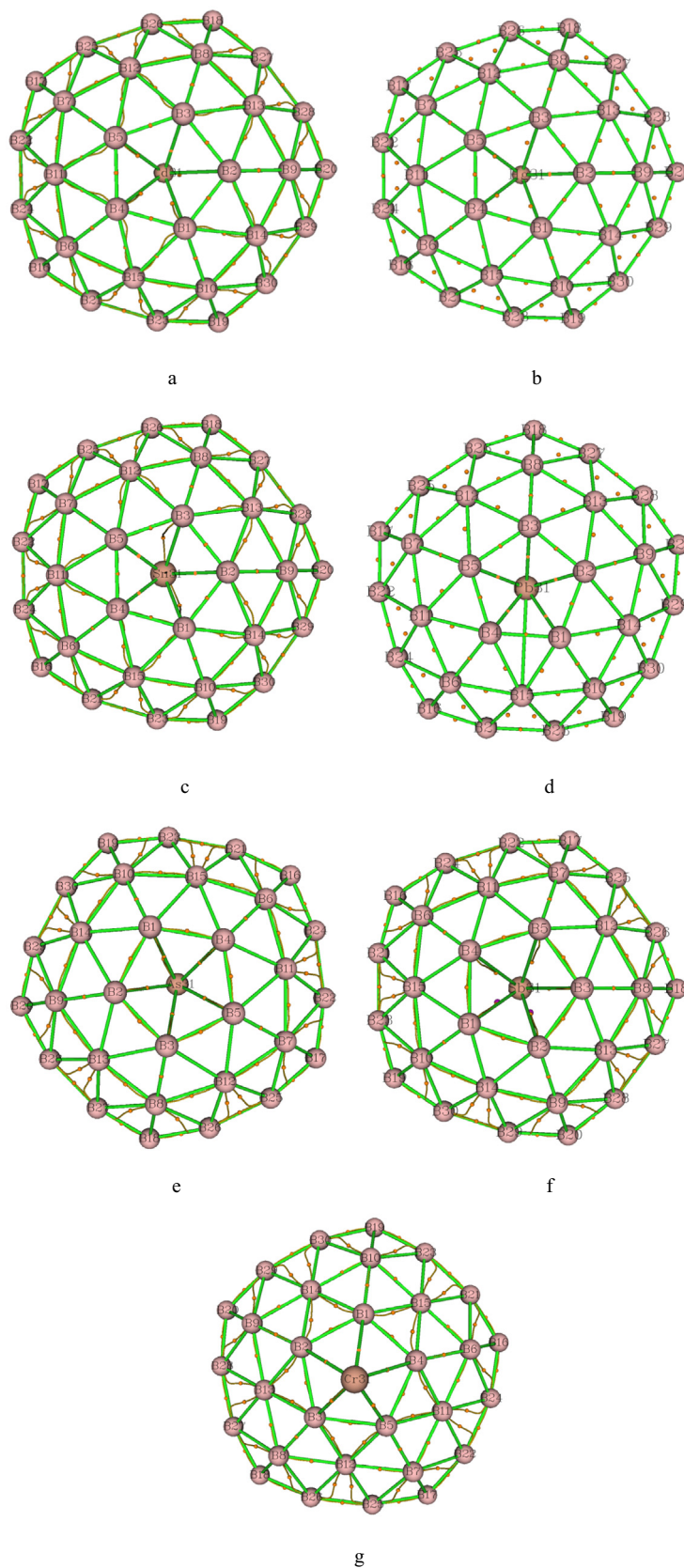
Fig. 8. Molecular graphs of a) Cd^{2+}/B_{30}, b) Hg^{2+}/B_{30}, c) Pb^{2+}/B_{30}, d) Sn^{2+}/B_{30}, e) As^{3+}/B_{30}, f) Sb^{3+}/B_{30}, and g) Cr^{3+}/B_{30} complexes in the aqueous media.

intermolecular bonds using the $\nabla^2\rho_b$ and H_b values [83–85]. Positive values of both $\nabla^2\rho_b$ and H_b signify a weak interaction, negative values of both $\nabla^2\rho_b$ and H_b denote a strong interaction, and a negative value of H_b with a positive value of $\nabla^2\rho_b$ refer to interactions with a medium strength. It can be seen from Table 7, As^{3+}/B_{30} complex shows strong interactions between the As^{3+} metal ion and

Table 7
The topological parameters at the BCP in a.u for M^{2+}/B_{30} and M^{3+}/B_{30} complexes in the aqueous media.

System	Bond	ρ_b	$\nabla^2\rho_b$	H_b	G_b	V_b	$G_b/|V_b|$
Cd^{2+}/B_{30}	M−B1	0.0587	0.119	−0.157	0.457	−0.614	0.744
	M−B2	0.0573	0.118	−0.144	0.440	−0.584	0.802
	M−B3	0.0548	0.111	−0.129	0.408	−0.538	0.758
	M−B4	0.0505	0.109	−0.998	0.374	−0.474	0.789
	M−B5	0.0600	0.126	−0.170	0.461	−0.631	0.730
Hg^{2+}/B_{30}	M−B1	0.0633	0.961	−0.204	0.648	−0.444	1.459
	M−B2	0.0616	0.967	−0.188	0.619	−0.430	1.439
	M−B3	0.0619	0.920	−0.171	0.572	−0.401	1.426
	M−B4	0.0217	0.971	−0.132	0.507	−0.375	1.352
	M−B5	0.0646	0.904	−0.218	0.663	−0.444	1.493
Pb^{2+}/B_{30}	M−B1	0.0381	0.842	−0.260	0.500	−0.310	1.612
	M−B2	0.0425	0.814	−0.292	0.593	−0.382	1.552
	M−B3	0.0431	0.847	−0.298	0.562	−0.384	1.463
	M−B4	0.0383	0.856	−0.262	0.511	−0.388	1.317
	M−B5	0.0430	0.862	−0.299	0.538	−0.383	1.404
Sn^{2+}/B_{30}	M−B1	0.0412	0.758	−0.278	0.585	−0.366	1.598
	M−B2	0.0416	0.794	−0.283	0.546	−0.367	1.487
	M−B3	0.0428	0.810	−0.289	0.540	−0.375	1.440
	M−B4	0.0456	0.833	−0.283	0.569	−0.382	1.489
	M−B5	0.0474	0.861	−0.295	0.562	−0.388	1.448
As^{3+}/B_{30}	M−B1	0.0683	− 0.730	−0.198	0.135	−0.377	0.358
	M−B2	0.0682	−0.295	−0.203	0.180	− 0.379	0.474
	M−B3	0.0678	−0.694	−0.101	0.139	−0.380	0.365
	M−B4	0.0681	−0.625	− 0.194	0.177	−0.372	0.475
	M−B5	0.0682	−0.806	−0.200	0.180	−0.381	0.472
Sb^{3+}/B_{30}	M−B1	0.0514	0.127	−0.242	0.274	−0.517	0.529
	M−B2	0.0512	0.108	−0.246	0.273	−0.520	0.525
	M−B3	0.0514	0.130	−0.237	0.269	−0.506	0.531
	M−B4	0.0512	0.136	−0.241	0.275	−0.516	0.532
	M−B5	0.0528	0.107	−0.246	0.273	−0.520	0.525
Cr^{3+}/B_{30}	M−B1	0.0716	0.111	−0.171	0.437	−0.665	0.657
	M−B2	0.0624	0.128	−0.148	0.468	−0.617	0.758
	M−B3	0.0733	0.108	−0.226	0.498	−0.724	0.687
	M−B4	0.0608	0.132	−0.138	0.469	−0.607	0.772
	M−B5	0.0702	0.114	−0.206	0.492	−0.699	0.703

bowl-like B_{30} nanosheet with negative sign of $\nabla^2\rho_b$ and H_b values whereas other complexes show medium interactions. It is worth noting that a non-covalent interaction will be observed for $(G_b/|V_b|) > 1$, electrostatic and covalent interactions will occur for $0.5 < G_b/|V_b| < 0$, and $1 < G_b/|V_b| < 0.5$, respectively [86]. The calculated $G_b/|V_b|$ amounts for the As − B bond are between 0 and 0.5, which mean that this bond is covalent in nature. A similar calculation has been performed for other bonds, which infers that Hg − B, Pb − B, and Sn − B bonds have non-covalent character whereas the nature of Cd − B, Sb − B, and Cr − B bonds is electrostatic and partially covalent.

4. Conclusion

DFT calculations were employed to evaluate the adsorption of Cd^{2+}, Hg^{2+}, Pb^{2+}, Sn^{2+}, As^{3+}, Sb^{3+}, and Cr^{3+} metal ions onto the surface of bowl-like B_{30} nanosheet. Our results showed that water as an aqueous media has a key role in the interaction between bowl-like B_{30} nanosheet and metal ions. Maximum adsorption of bowl-like B_{30} nanosheet was obtained for As^{3+} metal ion with the magnitude of −628.56 kcal mol^{-1} and minimum adsorption energy was found for Pb^{2+}, which was about −141.25 kcal mol^{-1} in the aqueous media. This confirmed that As^{3+} metal ion could create the strongest chemisorption with bowl-like B_{30} nanosheet in the aqueous media. The electronic properties of complexes were investigated and the results showed that E_g of bowl-like B_{30} nanosheet decreased considerably after adsorbing metal ions. The DOS spectra in the aqueous media confirmed that the most prominent decrease of E_g value was observed in the case of Cd^{2+}/B_{30} complex, showing the most sensitivity of bowl-like B_{30} nanosheet toward Cd^{2+} metal ion. Finally, QTAIM calculations showed that there are

strong interactions (covalent interactions) between As^{3+} metal ion and the bowl-like B_{30} nanosheet.

CRediT authorship contribution statement

Sadegh Kaviani: Formal analysis, Writing – original draft. **Dmitrii A. Tayurskii:** Supervision, Formal analysis, Writing – original draft. **Oleg V. Nedopekin:** Formal analysis, Writing – original draft. **Irina Piyanzina:** Writing – review & editing.

Declaration of Competing Interest

The authors declare that they have no known competing financial interests or personal relationships that could have appeared to influence the work reported in this paper.

Appendix A. Supplementary material

Supplementary data to this article can be found online at https://doi.org/10.1016/j.molliq.2022.120131.

References

[1] F.J. Osuna, E. Pavón, M.D. Alba, Pb^{2+}, Cd^{2+} and Hg^{2+} removal by designed functionalized swelling high-charged micas, Sci. Total Environ. 764 (2021) 142811.

[2] P.B. Tchounwou, C.G. Yedjou, A.K. Patlolla, D.J. Sutton, Heavy Metal Toxicity and the Environment. In Molecular, Clinical and Environmental Toxicology, Springer, 133–164, 2012.

[3] M. Ebrahimi, N. Khalili, S. Razi, M. Keshavarz-Fathi, N. Khalili, N. Rezaei, Effects of lead and cadmium on the immune system and cancer progression, J. Environ. Health Sci. 18 (2020) 335–343.

[4] S. Mitra, A.J. Chakraborty, A.M. Tareq, T.B. Emran, F. Nainu, A. Khusro, A.M. Idris, M.U. Khandaker, H. Osman, F.A. Alhumaydhi, Impact of heavy metals on the environment and human health: novel therapeutic insights to counter the toxicity, J. King Saud Univ. Sci. 34 (2022) 101865.

[5] S.F. Ahmed, P.S. Kumar, M.R. Rozbu, A.T. Chowdhury, S. Nuzhat, N. Rafa, T.M.I. Mahlia, H.C. Ong, M. Mofijur, Heavy metal toxicity, sources, and remediation techniques for contaminated water and soil, Environ. Technol. Innov. 25 (2022) 102114.

[6] L. Shi, Y. Yuan, Y. Xiao, P. Long, W. Li, Y. Yu, Y. Liu, K. Liu, H. Wang, L. Zhou, Associations of plasma metal concentrations with the risks of all-cause and cardiovascular disease mortality in Chinese adults, Environ. Int. 157 (2021) 106808.

[7] T.A. Saleh, M. Mustaqeem, M. Khaled, Water treatment technologies in removing heavy metal ions from wastewater: a review, Environmental Environ. Nanotechnol. Monit. Manag. 17 (2022) 100617.

[8] C.H. Yun, R. Prasad, A.K. Guha, K.K. Sirkar, Hollow fiber solvent extraction removal of toxic heavy metals from aqueous waste streams, Ind. Eng. Chem. Res. 32 (6) (1993) 1186–1195.

[9] Y.D. Zou, X.X. Wang, Z.S. Chen, W. Yao, Y.J. Ai, Y.H. Liu, T. Hayat, A. Alsaedi, N.S. Alharbi, X.K. Wang, Superior coagulation of graphene oxides on nanoscale layered double hydroxides and layered double oxides, Environ. Pollut. 219 (2016) 107–117.

[10] A. Bashir, L.A. Malik, S. Ahad, T. Manzoor, M.A. Bhat, G.N. Dar, A.H. Pandith, Removal of heavy metal ions from aqueous system by ion-exchange and biosorption methods, Environ. Chem. Lett. 17 (2) (2019) 729–754.

[11] B.H. Xie, C. Shan, Z. Xu, X.C. Li, X.L. Zhang, J.J. Chen, B.C. Pan, One-step removal of Cr(VI) at alkaline pH by UV/sulfite process: reduction to Cr(III) and in situ Cr (III) precipitation, Chem. Eng. J. 308 (2017) 791–797.

[12] T.S. Vo, M.M. Hossain, H.M. Jeong, K. Kim, Heavy metal removal applications using adsorptive membranes, Nano Converg. 7 (2020) 1–17.

[13] H.K. Patel, R.K. Kalaria, P.H. Jokhakar, C.R. Patel, B.Y. Patel, in: Development in Wastewater Treatment Research and Processes, Elsevier, 2022, pp. 385–400, https://doi.org/10.1016/B978-0-323-85583-9.00005-3.

[14] A. Ali, A. Mannan, I. Hussain, I. Hussain, M. Zia, Effective removal of metal ions from aqueous solution by silver and zinc nanoparticles functionalized cellulose: Isotherm, kinetics and statistical supposition of process, Environ. Nanotechnol. Monit. Manag. 9 (2018) 1–11.

[15] F. Karimi, A. Ayati, B. Tanhaei, A.L. Sanati, S. Afshar, A. Kardan, Z. Dabirifar, C. Karaman, Removal of metal ions using a new magnetic chitosan nano-bio-adsorbent; a powerful approach in water treatment, Environ. Res. 203 (2022) 111753.

[16] R. Chakraborty, A. Asthana, A.K. Singh, B. Jain, A.B.H. Susan, Adsorption of heavy metal ions by various low-cost adsorbents: a review, Int. J. Environ. Anal. Chem. 102 (2) (2022) 342–379.

[17] Y. Luo, L. Ou, J. Chen, G. Zhang, Y. Xia, B. Zhu, H. Zhou, A DFT study of the Pb ion adsorption on smithsonite (1 0 1) surface in aqueous system, J. Mol. Liq. 342 (2021) 117560.

[18] Y. Luo, L. Ou, J. Chen, G. Zhang, Y. Xia, B. Zhu, H. Zhou, Atomic-level insights into the modification mechanism of Fe (III) ion on smithsonite (1 0 1) surface from DFT calculation, Adv. Powder Technol. 33 (2022) 103695.

[19] Y. Luo, L. Ou, J. Chen, G. Zhang, Y. Xia, B. Zhu, H. Zhou, Mechanism insights into the hydrated Al ion adsorption on talc (001) basal surface: a DFT study, Surf. Interfaces. 30 (2022) 101973, https://doi.org/10.1016/j.surfin.2022.101973.

[20] J. Yang, B. Hou, J. Wang, B. Tian, J. Bi, N. Wang, X. Li, X. Huang, Nanomaterials for the removal of heavy metals from wastewater, Nanomaterials. 9 (2019) 424.

[21] T.V.J. Charpentier, A. Neville, J.L. Lanigan, R. Barker, M.J. Smith, T. Richardson, Preparation of magnetic carboxymethylchitosan nanoparticles for adsorption of heavy metal ions, ACS omega. 1 (1) (2016) 77–83.

[22] A. Razzaz, S. Ghorban, L. Hosayni, M. Irani, M. Aliabadi, Chitosan nanofibers functionalized by TiO_2 nanoparticles for the removal of heavy metal ions, J. Taiwan Inst. Chem. Eng. 58 (2016) 333–343.

[23] V.B. Arce, R.M. Gargarello, F. Ortega, V. Romañano, M. Mizrahi, J.M. Ramallo-López, C.J. Cobos, C. Airoldi, C. Bernardelli, E.R. Donati, D.O. Mártire, EXAFS and DFT study of the cadmium and lead adsorption on modified silica nanoparticles, Spectrochim Acta A. Mol. Biomol. Spectrosc. 151 (2015) 156–163.

[24] V. Madhavi, A.V.B. Reddy, G. Madhavi, Nanosorbents for the removal of heavy metal pollutants, in Nano-Bioremediation: Fundamentals and Applications, 363–387, Elsevier, 2022.

[25] M. Li, G. Huang, X. Chen, J. Yin, P. Zhang, Y. Yao, J. Shen, Y. Wu, J. Huang, Perspectives on environmental applications of hexagonal boron nitride nanomaterials, Nano Today. 44 (2022) 101486.

[26] Y. Cao, H.A. Dhhad, H.M. Hussen, A.E. Anqi, N. Farouk, A. Issakhov, N.Y. Xu, Z. Wei, Adsorption properties of two-dimensional carbon material towards the heavy metal ions, J. Mol. Liq. 342 (2021) 117500.

[27] K. Wang, D.Z. Li, R. Li, L.Y. Feng, Y.J. Wang, H. Jin, Zhai, Concentric dual π aromaticity in bowl-like B_{30} cluster: an all-boron analogue of corannulene, Phys. Chem. Chem. Phys. 18 (2016) 23304–23311.

[28] W.L. Li, R. Pal, Z.A. Piazza, X.C. Zeng, L.S. Wang, B27⁻: Appearance of the smallest planar boron cluster containing a hexagonal vacancy, J. Chem. Phys. 142 (2015) 204305.

[29] W.-L. Li, Y.-F. Zhao, H.-S. Hu, J. Li, L.-S. Wang, $[B_{30}]^-$: a quasiplanar chiral boron cluster, Angew. Chem. Int. Ed. 53 (22) (2014) 5540–5545.

[30] L. Li, J. Zhao Defected boron nitride nanosheet as an electronic sensor for 4-aminophenol: a density functional theory study, J. Mol. Liq. 306 (2020) 112926.

[31] X. Li, S. Chen, Q. Liu, Y. Luo, X. Sun, Hexagonal boron nitride nanosheet as an effective nanoquencher for the fluorescence detection of microRNA, Chem, Commun. 57 (2021) 8039–8042.

[32] S.S. Dindorkar, R.V. Patel, A. Yadav, Quantum chemical study of the defect laden monolayer boron nitride nanosheets for adsorption of pesticides from wastewater, Colloids Surfaces A: Physicochem. Eng. Asp. 643 (2022) 128795, https://doi.org/10.1016/j.colsurfa.2022.128795.

[33] A. Yadav, S.S. Dindorkar, Adsorption behaviour of hexagonal boron nitride nanosheets towards cationic, anionic and neutral dyes: insights from first principle studies, Colloids Surfaces A: Physicochem. Eng. Asp. 640 (2022) 128509, https://doi.org/10.1016/j.colsurfa.2022.128509.

[34] A. Yadav, S.S. Dindorkar, S.B. Ramisetti, N. Sinha, Sinha Simultaneous adsorption of methylene blue and arsenic on graphene, boron nitride and boron carbon nitride nanosheets: Insights from molecular simulations, J. Water Process Eng. 46 (2022) 102653, https://doi.org/10.1016/j.jwpe.2022.102653.

[35] Y.-G. Park, S.-N. Nam, M. Jang, C. Min Park, N. Her, J. Sohn, J. Cho, Y. Yoon, Boron nitride-based nanomaterials as adsorbents in water: a review, Sep. Purif. Technol. 288 (2022) 120637, https://doi.org/10.1016/j.seppur.2022.120637.

[36] B. Chettri, P.K. Patra, N.N. Hieu, D.P. Rai, Hexagonal boron nitride (h-BN) nanosheet as a potential hydrogen adsorption material: a density functional theory (DFT) study Surf, Interfaces. 24 (2021) 101043.

[37] J. Azamat, A. Khataee, S.W. Joo, Separation of copper and mercury as heavy metals from aqueous solution using functionalized boron nitride nanosheets: a theoretical study, J. mol.struct. 1108 (2016) 144–149.

[38] F. Han, Y. Zong, D. Jassby, J. Wang, J. Tian, The interactions and adsorption mechanisms of ternary heavy metals on boron nitride, Environ. Res. 183 (2020) 109246.

[39] Milon, M.K. Hossain, D. Roy, F. Ahmed, Ahmed, Boron nanocluster as a heavy metal adsorbent in aqueous environment: a DFT Study, J. Mol. Struct. 1237 (2021) 130302, https://doi.org/10.1016/j.molstruc.2021.130302.

[40] J. Li, P. Jin, W. Dai, C.H. Wang, R. Li, T. Wu, C.C. Tang Excellent performance for water purification achieved by activated porous boron nitride nanosheets, Mater. Chem. Phys. 196 (2017) 186–193.

[41] J. Azamat, J.J. Sardroodi, L. Poursoltani, D. Jahanshahi, Functionalized boron nitride nanosheet as a membrane for removal of Pb^{2+} and Cd^{2+} ions from aqueous solution, J. Mol. Liq. 321 (2021) 114920.

[42] Z. Noroozi, R. Rahimi, M. Solimannejad, A computational study for the B_{30} bowllike nanostructure as a possible candidate for drug delivery system for amantadine, Comput. Theor. Chem. 1129 (2018) 9–15.

[43] R. Rahimi, M. Solimannejad, Can bowl-like B_{30} nanostructure sense toxic cyanogen gas in air?: a theoretical study, Mol. Phys. 116 (2018) 2196–2204.

[44] M.J. Frisch, G.W. Trucks, H.B. Schlegel, G.E. Scuseria, M.A. Robb, J.R. Cheeseman, G. Scalmani, V. Barone, G.A. Petersson, H. Nakatsuji, X. Li, M. Caricato, A.V. Marenich, J. Bloino, B.G. Janesko, R. Gomperts, B. Mennucci, H.P. Hratchian, J.V. Ortiz, A.F. Izmaylov, J.L. Sonnenberg, Williams, F. Ding, F. Lipparini, F. Egidi, J. Goings, B. Peng, A. Petrone, T. Henderson, D. Ranasinghe, V.G. Zakrzewski, J. Gao, N. Rega, G. Zheng, W. Liang, M. Hada, M. Ehara, K. Toyota, R. Fukuda, J. Hasegawa, M. Ishida, T. Nakajima, Y. Honda, O. Kitao, H. Nakai, T. Vreven, K. Throssell, J.A. Montgomery Jr., J.E. Peralta, F. Ogliaro, M.J. Bearpark, J.J. Heyd, E. N. Brothers, K.N. Kudin, V.N. Staroverov, T.A. Keith, R. Kobayashi, J. Normand, K. Raghavachari, A.P. Rendell, J.C. Burant, S.S. Iyengar, J. Tomasi, M. Cossi, J.M. Millam, M. Klene, C. Adamo, R. Cammi, J.W. Ochterski, R.L. Martin, K. Morokuma, O. Farkas, J.B. Foresman, D.J. Fox, Wallingford, CT, 2016.

[45] S.U.D. Shamim, M.H. Miah, M.R. Hossain, M.M. Hasan, M.K. Hossain, Hossain Md Abul, Ahmed Farid, Theoretical investigation of emodin conjugated doped $B_{12}N_{12}$ nanocage by means of DFT, QTAIM and PCM analysis, Physica E Low Dimens. Syst. Nanostruct. 136 (2022) 115027.

[46] S. Shafiq, R.A. Shehzad, M. Yaseen, K. Ayub, A.R. Ayub, J. Iqbal, K.H. Mahmoud, Z.M. El-Bahy, DFT study of OLi_3 and MgF_3 doped boron nitride with enhanced nonlinear optical behavior, J. Mol. Struct. 1251 (2022) 131934.

[47] F. Kamali, G. Ebrahimzadeh-Rajaei, S. Mohajeri, A. Shamel, M. Khodadadi-Moghaddam, A computational design of $X_{24}Y_{24}$ (X= B, Al, and Y= N, P) nanoclusters as effective drug carriers for metformin anticancer drug: a DFT insight, Inorg. Chem. Commun. 141 (2022) 109527.

[48] A.U. Khan, S. Muhammad, R.A. Khera, R.A. Shehzad, K. Ayub, J. Iqbal, DFT study of superhalogen (AlF₄) doped boron nitride for tuning their nonlinear optical properties, Optik. 231 (2021) 166464.

[49] H. Zhu, J. Yuan, X. Tan, W. Zhang, M. Fang, X. Wang, Efficient removal of Pb^{2+} by Tb-MOFs: identifying the adsorption mechanism through experimental and theoretical investigations, Environ. Sci. Nano. 6 (2019) 261–272.

[50] A.A. Menazea, H.A. Ezzat, W. Omara, O.H. Basyouni, S.A. Ibrahim, A.A. Mohamed, W. Tawfik, M.A. Ibrahim, Chitosan/graphene oxide composite as an effective removal of Ni, Cu, As, Cd and Pb from wastewater, Comput. Theor. Chem. 1189 (2020) 112980.

[51] M. Guin, J.B. Singh, A. Sharma, S.B. Elavarasi, Density functional theory investigation of triazole substituted nitro borazine derivatives as high energy

density material, Mater. Today: Proc. (2022), https://doi.org/10.1016/j.matpr.2022.06.200.

[52] R. Jindal, V. Sharma, A. Shukla, Density functional theory study of the hydrogen evolution reaction in haeckelite boron nitride quantum dots, Int. J. Hydrog. Energy. (2022), https://doi.org/10.1016/j.ijhydene.2022.06.216.

[53] Y. Cao, S. Alamri, A.A. Rajhi, A.E. Anqi, M. Derakhshandeh, The capability of boron carbide nanotube as a nanocarrier for fluorouracil anticancer drug delivery; DFT study, Mater. Chem. Phys. 275 (2022) 125260.

[54] J.A. Sordo, S. Chin, T.L. Sordo, On the counterpoise correction for the basis set superposition error in large systems, Theor. Chim. Acta. 74 (2) (1988) 101–110.

[55] J. Tomasi, B. Mennucci, R. Cammi, Quantum mechanical continuum solvation models, Chem. Rev. 105 (8) (2005) 2999–3094.

[56] Y.A. Atia, D.O. Bokov, K.R. Zinnatullovich, M.M. Kadhim, W. Suksatan, W.K. Abdelbasset, H.A. Hammoodi, Y.F. Mustafa, Y. Cao, The role of amino acid functionalization for improvement of adsorption Thioguanine anticancer drugs on the boron nitride nanotubes for drug delivery, Mater. Chem. Phys. 278 (2022) 125664.

[57] T. Koopmans, Über die Zuordnung von Wellenfunktionen und Eigenwerten zu den Einzelnen Elektronen Eines Atoms, Physica. 1 (1-6) (1934) 104–113.

[58] R.G. Pearson, Chemical hardness and density functional theory, J. Chem. Sci. 117 (5) (2005) 369–377.

[59] A.E. Reed, R.B. Weinstock, F. Weinhold, Natural population analysis, J. Chem. Phys. 83 (1985) 735–746.

[60] S. Dapprich, G. Frenking, Investigation of Donor-Acceptor Interactions: a Charge Decomposition Analysis Using Fragment Molecular Orbitals, J. Phys. Chem. 99 (1995) 9352–9362.

[61] R.F.W. Bader, A quantum theory of molecular structure and its applications, Chem. Rev. 91 (5) (1991) 893–928.

[62] T. Lu, F. Chen, Multiwfn: a multifunctional wavefunction analyzer, J. Comput. Chem. 33 (2012) 580–592.

[63] F. Furche, R. Ahlrichs, Adiabatic time-dependent density functional methods for excited state properties, J. Chem. Phys. 117 (16) (2002) 7433–7447.

[64] R. Bauernschmitt, R. Ahlrichs, Treatment of electronic excitations within the adiabatic approximation of time dependent density functional theory, Chem. Phys. Lett. 256 (4-5) (1996) 454–464.

[65] L. Gontrani, O. Pulci, M. Carbone, R. Pizzoferrato, P. Prosposito, Detection of heavy metals in water using graphene oxide quantum dots: an experimental and theoretical study, Molecules. 26 (2021) 5519.

[66] A.D. Tamafo Fouegue, J.H. Nono, N.K. Nkungli, J.N. Ghogomu, A theoretical study of the structural and electronic properties of some titanocenes using DFT, TD-DFT, and QTAIM, Struct. Chem. 32 (1) (2021) 353–366.

[67] R. Bhuvaneswari, V. Nagarajan, R. Chandiramouli, Physisorption of propane and butane vapors on novel Kagome antimonene sheets e a first-principles perception Chem, Phys. Lett. 754 (2020) 137693.

[68] T. Jadoon, T. Mahmood, K. Ayub, Silver cluster (Ag$_6$) decorated coronene as non-enzymatic sensor for glucose and H$_2$O$_2$, J. Mol. Graph. Model. 103 (2021) 107824.

[69] R. Bhuvaneswari, V. Nagarajan, R. Chandiramouli, Red tricycle phosphorene nanoribbon as a removing medium of sulfadiazine and sulfamethoxazole molecules based on first-principles studies, J. Mol. Liq. 336 (2021) 116294.

[70] M.H. Mohammed, B.A. Jarullah, F.H. Hanoon, Using of cellulose with various nanoparticles as chelating factors in nanovaccines: Density functional theory investigations, Solid State Commun. 316-317 (2020) 113945, https://doi.org/10.1016/j.ssc.2020.113945.

[71] M.R. Hossain, M.M. Hasan, F. Nishat Maliha, T. Ahmed, M.A.H. Ferdous, DFT and QTAIM investigations of the adsorption of chlormethine anticancer drug on the exterior surface of pristine and transition metal functionalized boron nitride fullerene, J. Mol. Liq. 323 (2021) 114627.

[72] A. Soltani, M.T. Baei, M. Mirarab, M. Sheikhi, E. Tazikeh Lemeski, The electronic and structural properties of BN and BP nano-cages interacting with OCN⁻: a DFT study, J. Phys. Chem. Solids. 75 (10) (2014) 1099–1105.

[73] F. Weinhold, C.R. Landis, Natural bond orbitals and extensions of localized bonding concepts, Chem. Educ. Res. Pract. 2 (2) (2001) 91–104.

[74] M. Doust Mohammadi, The adsorption of 1-Chloro-1,2,2,2-tetrafluoroethane onto the pristine, Al-, and Ga-doped boron nitride nanosheet H. Y. Abdullah, Theor. Chem. Acc. 139 (2020) 1–17.

[75] A.M.F. Costa, S.Q. de Aguiar Filho, T.J. Santos, D.H. Pereira, Theoretical insights about the possibility of removing Pb^{2+} and Hg^{2+} metal ions using adsorptive processes and matrices of carboxymethyl diethylaminoethyl cellulose and cellulose nitrate biopolymers, J. Mol. Liq. 331 (2021) 115730.

[76] Y. Gao, F. Xu, J. Wu, H. Zhao, A.G. Ebadi, Detection and adsorption of cathinone drug by magnesium oxide nanostructure: DFT study, Comput. Theor. Chem. 1207 (2022) 113507, https://doi.org/10.1016/j.comptc.2021.113507.

[77] J.S. Al-Otaibi, Y.S. Mary, Y.S. Mary, R. Trivedi, B. Chakrabory, R. Thomas, Cluster formation between an oxadiazole derivative with metal nanoclusters (Ag/Au/Cu), graphene quantum dot sheets, SERS studies and solvent effects, Appl. Surf. Sci. 146758 (2020) 1–30.

[78] I. Shtepliuk, N.M. Caffrey, T. Iakimov, V. Khranovskyy, I.A. Abrikosov, R. Yakimova, On the interaction of toxic Heavy Metals (Cd, Hg, Pb) with graphene quantum dots and infinite graphene, Sci. Rep. 7 (2017) 1–17.

[79] H. Xu, Q. Wang, G. Fan, X. Chu, Theoretical study of boron nitride nanotubes as drug delivery vehicles of some anticancer drugs, Theor. Chem. Acc. 137 (2018) 1–15.

[80] N.K. Hien, N.C. Bao, N.T.A. Nhung, N.T. Trung, P.C. Nam, Duong Tran, J. S. Kim, D. T. Quang, A highly sensitive fluorescent chemosensor for simultaneous determination of Ag (I), Hg (II), and Cu (II) ions: Design, synthesis, characterization and application, Dyes Pigm. 116 (2015) 89–96.

[81] N. Chetry, T.G. Devi, T. Karlo, Synthesis and characterization of metal complex amino acid using spectroscopic methods and theoretical calculation, J. Mol. Struct. 1250 (2022) 131670.

[82] K.S. Mani, R. Rajamanikandan, B. Murugesapandian, R. Shankar, G. Sivaraman, M. Ilanchelian, S.P. Rajendran, Coumarin based hydrazone as an ICT-based fluorescence chemosensor for the detection of Cu^{2+} ions and the application in HeLa cells, Spectrochim. Acta A Mol. Biomol. Spectrosc. 214 (2019) 170–176.

[83] A. Mortazavifar, H. Raissi, A. Akbari, DFT and MD investigations on the functionalized boron nitride nanotube as an effective drug delivery carrier for Carmustine anticancer drug, J. Mol. Liq. 276 (2019) 577–587.

[84] M.R. Hossain, M.M. Hasan, N.-E. Ashrafi, H. Rahman, M.S. Rahman, F. Ahmed, T. Ferdous, M.A. Hossain, Adsorption behaviour of metronidazole drug molecule on the surface of hydrogenated graphene, boron nitride and boron carbide nanosheets in gaseous and aqueous medium: a comparative DFT and QTAIM insight, Physica E Low Dimens. Syst. Nanostruct. 126 (2021) 114483, https://doi.org/10.1016/j.physe.2020.114483.

[85] P. Khan, M. Jamshaid, S. Tabassum, S. Perveen, T. Mahmood, K. Ayub, J. Yang, M.A. Gilani, Exploring the interaction of ionic liquids with Al$_{12}$N$_{12}$ and Al$_{12}$P$_{12}$ nanocages for better electrode-electrolyte materials in super capacitors, Journal of Molecular Liquids, J. Mol. Liq. 344 (2021) 117828.

[86] M. Khavani, M. Izadyar, M.R. Housaindokht, DFT investigation and molecular dynamic simulation on the selective complexation of cis-cyclic nanopeptides with alkaline earth metal ions, Sens. Actuators B Chem. 221 (2015) 1120–1129.